EUROFUSION WPJET1-CP(16) 15337

U Hoefel et al.

Confinement in Wendelstein 7-X Limiter Plasmas

Preprint of Paper to be submitted for publication in
Proceedings of 26th IAEA Fusion Energy Conference

This work has been carried out within the framework of the EUROfusion Consortium and has received funding from the Euratom research and training programme 2014-2018 under grant agreement No 633053. The views and opinions expressed herein do not necessarily reflect those of the European Commission.

Confinement in Wendelstein 7-X Limiter Plasmas

M. Hirsch[1], A. Dinklage[1], A. Alonso[2], G. Fuchert[1], S. Bozhenkov[1], T. Andreeva[1], J. Baldzuhn[1], M. Beurskens[1], H.-S. Bosch[1], C.D. Beidler[1], C. Biedermann[1], E. Blanco[2], R. Brakel[1], R. Burhenn[1], B. Buttenschön[1], A. Cappa[2], A. Czarnecka[3], M. Endler[1], T. Estrada[2], T. Fornal[3], J. Geiger[1], O. Grulke[1], J.H. Harris[4], D. Hartmann[1], U. Höfel[1], M. Jakubowski[1], T. Klinger[1], S. Klose[1], J. Knauer[1], G. Kocsis[5], R. König[1], P. Kornejew[1], A. Krämer-Flecken[6], N. Krawczyk[3], M. Krychowiak[1], M. Kubkowska[3], I. Ksiazek[7], A. Langenberg[1], H.P. Laqua[1], S. Lazerson[8], H. Maaßberg[1], N. Marushchenko[1], S. Marsen[1], V. Moncada[9], D. Moseev[1], D. Naujoks[1], M. Otte[1], N. Pablant[8], E. Pasch[1], F. Pisano[10], K. Rahbarnia[1], T. Schröder[1], T. Stange[1], L. Stephey[11], T. Szepesi[5], T. Sunn Pedersen[1], H. Trimino Mora[1], H. Thomsen[1], H. Tsuchiya[12], Yu. Turkin[1], T. Wauters[13], U. Wenzel[1], A. Werner[1], R. Wolf[1], G.A. Wurden[14], D. Zhang[1] and the W7-X Team

[1] Max-Planck-Institut für Plasmaphysik, Greifswald, Germany
[2] CIEMAT, Madrid, Spain
[3] IPPLM, Warsaw, Poland
[4] Oak Ridge National Laboratory, Oak Ridge, TN, USA
[5] Wigner Institute, Budapest, Hungary
[6] Forschungszentrum Jülich, Jülich, Germany
[7] Opole University, Opole, Poland
[8] Princeton Plasma Physics Laboratory, Princeton, NJ, USA
[9] CEA Cadarache, France and THERMADIAG
[10] University of Cagliari, Cagliari, Italy
[11] University of Wisconsin, Madison, WI, USA
[12] National Institute for Fusion Science, Toki, Japan
[13] Laboratory for Plasma Physics, ERM-KMS, Brussels, Belgium, TEC Partner
[14] Los Alamos National Laboratory, Los Alamos, NM, USA

E-mail contact of main author: matthias.hirsch@ipp.mpg.de

Abstract. Observations on confinement in the first experimental campaign on the optimized Stellarator Wendelstein 7-X are summarized. In this phase W7-X was equipped with five inboard limiters only and thus the discharge length restricted to avoid local overheating. Stationary plasmas are limited to low densities < 2 to $3 \cdot 10^{19}$ m^{-3}. With the available 4.3 MW ECR heating core T_e~ 8 keV, T_i ~ 1 to 2 keV are achieved routinely resulting in energy confinement time τ_E between 100 to 150ms. For these conditions the plasmas show characteristics of core electron root confinement with peaked T_e-profiles and positive E_r up to about half of the minor radius. Profiles and plasma currents respond to on- and off-axis heating and co- and counter ECCD respectively.

1. Introduction

The mission of the superconducting Wendelstein 7-X (W7-X) is to explore the capability of optimized stellarators (1) as a route towards fusion energy. W7-X is based on the concept of helical-axis advanced stellarators (HELIAS) and aims at steady-state operation at reactor-relevant collisionality and plasma β. The project is conducted in a staged approach: In the first operational phase physics studies of the HELIAS properties will be performed including the exploration of a path towards a reactor-relevant divertor-compatible high-density regime. This phase will use a test divertor unit geometrically identical to the later steady-state divertor

but inertially cooled and thus with a lower risk of damage due to local overheating. The maximum absorbed heating power may be 80 MJ considering e.g. a discharge length of 10s at 8 MW ECRH. In a second phase with fully cooled steady-state divertor and hardened in-vessel components will extend the plasma duration to quasi steady-state discharges at high-performance conditions (the technical limit is given by the availability of cooling for 30 minutes). Prior to the physics exploration a test phase has been performed with graphite limiters only and yet unprotected metal wall dedicated to integrated commissioning and tests of components, diagnostics and device control (2). During the campaign more than 20 diagnostics were successfully commissioned and provided physics information such that a physics program could be conducted beyond tests as far as the machine conditions and diagnostic availability allowed. This paper gives an overview of the energy- and particle confinement in this first limiter phase of the W7-X project.

2. Expectations on confinement in W7-X

The magnetic field structure of a HELIAS minimizes the inherent drawbacks of classical non-axisymmetric confinement - namely unacceptable high collisionless transport in the reactor relevant long mean free path *lmfp* regime, unacceptable orbit losses of fast (heating) particles and a degradation of the flux surfaces at high β - while keeping the capability for steady state operation. This is simultaneously achieved by a poloidal closure of the contours of the second adiabatic invariant J - so called isodynamicity - resembling a minimization of the poloidal variation of $|B|$ (1). This reduces the radial component of the ∇B-drift and thus the neoclassical particle and energy transport in the *lmfp* regime, but also minimizes simultaneously the Pfirsch–Schlüter currents and thus the pressure induced Shafranov shift such that the selected optimized field structure becomes largely independent of β. Moreover, the bootstrap current and thus the free energy can be minimized with benefits for MHD stability the absence of disruptions. As the second characteristic element of the HELIAS concept, configurations with intrinsically low magnetic shear have been selected where the profile of the rotational transform can be chosen such that low order rationals and islands are avoided in the confinement region but may be used as an inherent diverting structures at its boundary. This island divertor (3) is rather sensitive to asymmetries of the magnetic field or of plasma facing components and thus relies on configuration control which becomes possible only by the successful minimization of plasma currents in a HELIAS. Some elements of this optimization path have been explored already in the predecessor Wendelstein 7-AS (4). Others, e.g. the influence of the selected magnetic configuration on turbulent transport as well as engineering aspects of a HELIAS have not yet been design criteria of W7-X.

Due to the lack of a disruptive density limit the stellarator route to a rector allows for high-density operation at comparatively moderate temperatures in accordance with divertor needs. Correspondingly high-density steady-state heating scenarios, such as ECRH O2-mode heating, need to be developed. High density scenarios at W7-AS and LHD already showed favorable good particle and energy confinement and even findings of a reduced impurity confinement which prevented accumulation.

The radial electric field E_r plays a particular role for stellarator confinement: In addition to isodynamic optimization, the high transport coefficients in the *lmfp* $1/\nu$ regime in a reactor core may be further reduced by $E_r x B$ rotation which leads to a de-trapping of the transport carrying trapped particles in the so-called $\sqrt{\nu}$ -regime. As the neoclassical electron- and ion-fluxes depend explicitly on E_r the ambipolarity condition of the radial fluxes may allow for multiple solutions (roots) of neoclassical electron- and ion-fluxes: In the ion-root for $T_e \sim T_i$, e.g. at plasma edge conditions, the strong outward thermodiffusion of the ions is reduced by

inward fluxes due to negative values of E_r. In contrast for regions with $T_e >> T_i$ (as for centrally heated ECRH discharges) the resulting strong electron fluxes are reduced to the level of the ion fluxes by strong positive E_r constituting Core Electron Root Confinement (5). CERC characteristics at low density ECRH discharges - i.e. peaked T_e and flat T_i profiles together with a positive E_r allow the first comparison of transport and confinement in W7-X with its neoclassical predictions. As the peaked T_e -profiles provide pronounced pressure gradients deep in the plasma core, they also will be the first candidate to measure the Shafranov shift which as a further optimization criterion in W7-X should be reduced. Turbulent fluxes which are widely ambipolar may depend on this neoclassically determined E_r via *ExB* shear flows as well. Therefore transport and confinement in a stellarator could be governed by neoclassics even if anomalous / turbulent fluxes prevail the neoclassical ones, e.g. at the high collisionalities at the edge.

3. Test operation phase: technical boundaries and diagnostics

In its first operation phase (started in the end of 2015 for 10 weeks of plasma experiments) W7-X was equipped with only five uncooled, inboard graphite limiters. A magnetic configuration $\iota_a > 5/6$ with the 5/6 island chain shifted clearly into the plasma had been selected which avoids diverting island structures at the plasma edge (6). Only a small configuration variation was acceptable to minimize the risk of uncontrolled loads apart from the limiters. To avoid overheating the maximum allowed absorbed energy was set to 4MJ per experiment program - thus restricting the discharge length. Stationary discharge scenarios over 6s were achieved, however with P_{ECRH} lowered to 0.6MW due to this energy limit. For plasma breakdown and heating a total power of 4.3 MW ECRH was routinely available provided by 6 long-pulse 140 GHz gyrotrons (7).

The device was operated first with preprogrammed helium- or hydrogen gas injection but yet without feedback density control. For wall conditioning He glow discharges were used in periods without magnetic field. With magnetic field on, a temporary depletion of the walls from H was possible with He recovery discharges. Sequences of low power ECRH conditioning discharges have been performed as well. The global gas balance showed that in average about a factor of 4 more particles were pumped than injected, thus outgassing dominated the fueling throughout OP1.1 (8). The impurity content - intrinsic (O, C, N) and injected impurities (Ar, Ne, N) as well as traces of F, Cl, S_2, Fe and Cu increased with the discharge time since the last glow discharge until it limited plasma duration by radiation (9).

The discharge scenarios generally show a high degree of reproducibility of their temporal (time traces) as well as in spatial behavior (profiles). An example for a representative discharge with 3.8 MW heating power provided by 6 gyrotrons and an overall duration of 1.2 s is given in Fig. 1. Besides a H-prefill, the density is ramped up in successive gas pulses displayed by steps in the dispersion interferometer (10) signal $\bar{n}_e$ and reaches $2.5 \cdot 10^{19}$ m^{-3}. The diamagnetic energy signal W_{dia} is compensated for currents induced in the vessel by a set of coils nearby the diamagnetic loop that do not encircle the plasma (11). Maximum stored energy was W_{dia}~500kJ resulting in central β values with $\beta(0)$ ~2% at B=2.5 T. Due to the steep core pressure gradients VMEC code calculations already predict a Shafranov-shift of δ= 3.4 cm at the triangular shaped toroidal plane. This, however, could not yet be verified from the accuracy and mapping of the available diagnostic information. Plasma currents measured by Rogowski coils (11) increase throughout the experiment as both, the *L/R*-time that prevails the total current evolution and the resistive skin time indicative for the redistribution of the plasma shielding currents exceed the discharge length. The total current reached values up to ~2kA in maximum (after 1s of co-ECCD but could be suppressed to

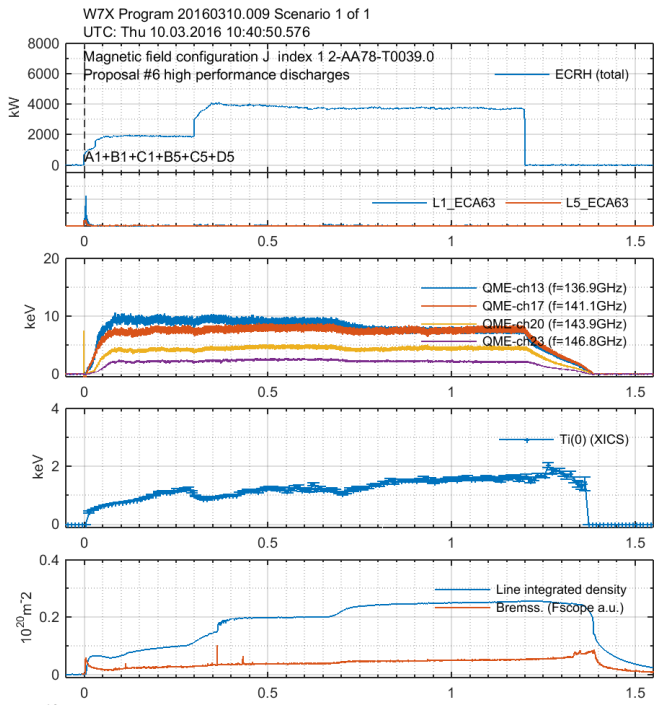

Fig. 1: Waveforms (from top to bottom) of heating power, selected ECE radiometer channels (13), central T_i derived from X-ray imaging spectroscopy (15) and line integrated density along a pathlength of 1.33m (10) for a W7-X discharge fuelled with a three subsequent hydrogen puffs.

0.1 kA with counter ECCD (12). A dipolar structure is observed as expected for a Pfirsch-Schlüter current pattern.

The electron temperature T_e was measured by a 32-channel absolutely calibrated ECE radiometer (13). T_e-profiles are derived from the X2 emission spectra taking into account the finite optical thickness. Further spectral components display the well known downshifted emission from higher-energetic thermal electrons in the plasma center for which the plasma is optically grey. T_e and n_e profile information is also obtained from Thomson scattering providing a half-profile of T_e and n_e with 10 channels at the outboard side including the limiter shadow (14). Raman scattering at Nitrogen is used for density calibration. An imaging X-ray spectrometer probing line integrated impurity spectra provided T_e profiles and the only T_i profile information via profile inversion - with highest accuracy especially at mid radii (15). A comparison of profiles is shown in Fig. 2:

In general, the T_e-profiles are highly reproducible for the same conditions, statistical errors play a minor role only and systematic errors from the diagnostic prevail. Stationary T_e profiles heated on axis show a hot core surrounded by steep temperature gradients around half minor radius resulting in about 8 keV in the center at P_{ECRH}= 4 MW. The T_i profile is rather flat with $T_i < T_e$ and a gradient zone outside r/a~0.5. Central T_i is increasing continuously unto the discharge end due to the increasing electron-ion coupling and reached up to 2 keV in the best cases (1.8 keV in Fig. 1). At densities up to the value $2 \cdot 10^{19}$ m^{-3} the T_e profiles remain almost stationary until heating termination as shown in the example of Fig. 1. For higher densities the discharge could not be maintained stationary with the available heating power rather than it is terminated by a radiation collapse starting from the plasma edge (16).

4. Observations on confinement in the limiter plasmas

4.1 Global energy confinement and power balance

From the T_e, T_i and n_e profiles the kinetic energy is calculated assuming Z_{eff}=1 due to unknown impurity content as $W_{kin} = (3/2)\int (n_e T_e + n_i T_i)(dV/dr)dr$. As a first step, the vacuum field is used for the mapping of the profiles and, hence, the calculation of dV/dr. The resulting W_{kin} exceeds the values from the compensated W_{dia} by 25% which is presumably due to the combined effect of Z_{eff}>1 and the mapping using vacuum fields (17). In general the ion energy content is $W_i \sim 1/3\ W_e$.

In the power balance $P_{ECRH} - P_{rad} - P_{CX} - P_{lim} = dW/dt$ the various components are (17):
P_{ECRH}, the heating power is measured with an accuracy of 10% in the transmission line and X2 absorption in the plasma is 95-97% as derived from EC absorption measurements (7).

P_{rad}, the radiative power loss derived from the first available two cameras of the bolometer assuming toroidal symmetry, is typically P_{rad}/P_{ECRH} = 25-40% for stationary conditions. This value increases with n_e and P_{ECRH} and depends on T_e and impurity concentration (16). For P_{ECRH} < 1MW a radiation dominated regime is found (19), further reduction finally leads to a radiation collapse. Generally the radiated fraction increases with integrated discharge time since the last glow discharge indicating increasing wall pollution.
P_{lim}, the power load to the limiter, estimated from two IR camera systems (18) indicates that at low ECRH power (0.6 MW) 60% is found in the limiters, this drops to 35% for 4MW.
Finally in the power balance ~10% of the P_{ECRH} are missing for P_{ECRH} < 1MW, a fraction which increases with heating power (17). This missing power may be due to the unknown contribution from CX-fluxes expected due to deep fuelling from the limiters which are located in a toroidal plane with maximum elongation such that due to the local flux compression they are geometrically close (~25cm) to the plasma axis. Another aspect are not yet identified limiter load asymmetries.

Derived energy confinement times are around ~100ms to 150ms and decrease with increasing radiated power fraction (19). Despite the poor wall conditions the energy confinement time already agrees with the stellarator scaling ISS04 (20).

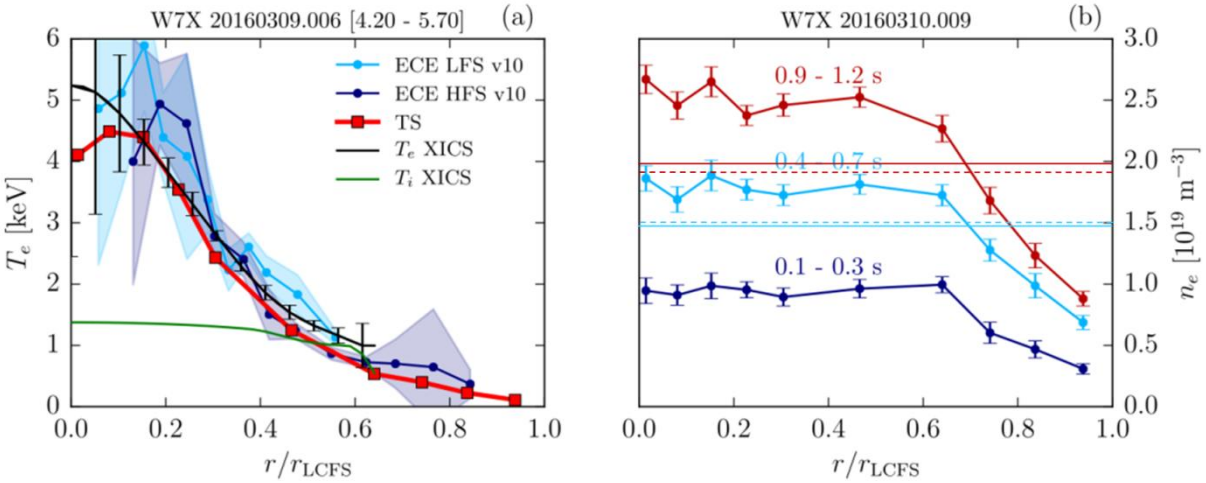

Fig. 2: Representative temperature and density profiles: Left: electron- and ion-temperature measured by ECE, Thomson scattering and X-ray imaging of Ar impurity lines. Error bars of ECE at low- and high-field side spectra resulting from absolute calibration uncertainties are shaded, the radial location is derived from the cold resonance. Thomson data plotted without error bars as systematic errors are being investigated; statistical errors are negligible. XICS error bars (black lines) represent inversion uncertainty. A low-beta plasma is shown (beta ?), as the profile comparison basses on vacuum configuration, the finite pressure Shafranov shift has not yet been included via the VMEC code. Right: Electron density measured by Thomson scattering during the build up phase of the plasma and two subsequent density steps. The resulting average densities are plotted as horizontal bars and compared with the value derived from interferometry. The limiter position LCFS corresponds to r_{eff}=50cm. Investigation of systematic errors and mapping of the diagnostic profile information is ongoing.

4.2 Particle and impurity confinement

The OP1.1 discharges suffered from a lack of density control and impurity influx. With He pulses in Hydrogen discharges an approach to particle confinement times is derived observing the decay of He II lines with a filterscope. The effective decay times τ_p* with values of 2 to 3 s depend on the magnetic configuration; shifting the 5/6 rational/islands inwards i.e. away from the fuelling zone increases the effective He decay time. The same holds for the fuelling efficiency displayed by the slope of the interferometer signals as a proxy (21). The determination of the true He confinement times τ_p are still under investigation.

First (upper) estimate on impurity confinement time τ_I is derived from the decay of the Ar impurity concentration in H discharges with Ar-prefill using data sufficiently late that ionization is completed and the temporal behavior should only reflect the confinement of Ar interfering with a certain recycling flux. Values of τ^*=150-300ms are found for highly ionized >ArXV near the center and >>1s for ionization states at the edge (15).

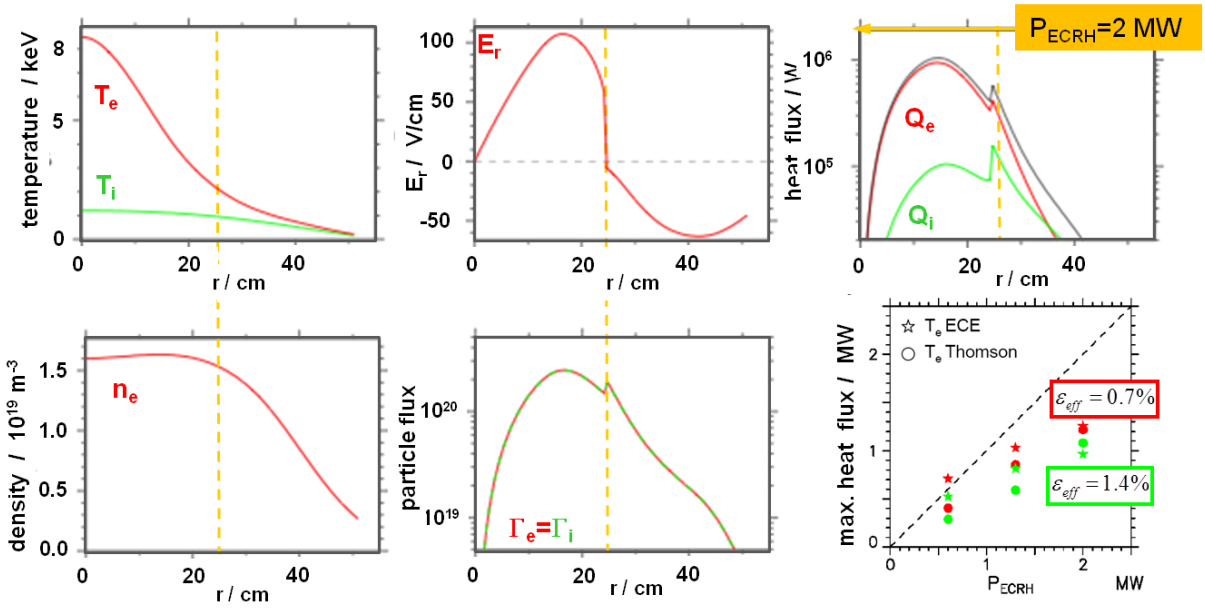

Fig. 3: Fits to temperature and density profiles (left column), derived ambipolar particle fluxes, resulting radial electric field (middle) and (upper right) electron and ion heat fluxes for a discharge with 2MW ECRH calculated with DKES (22) code assuming Z_{eff}=1. The gap between the maximum neoclassical heat flux and the heating power deposit in the center increases with P_{ECRH} (lower right).

4.3 Local transport analysis and comparison with neoclassical expectations

Energy ($Q_{e,i}$) and particle fluxes ($\Gamma_{e,i}$) integrated over the flux surfaces were derived from fits to the temperature and density profiles (Fig. 3). The peaked T_e profile together with flat $T_i(r)$ profiles where $T_i(0) << T_e(0)$ as shown in **Fig. 2:** indicate CERC conditions. From the ambipolarity condition, $\Gamma_e=\Gamma_i$, a positive radial electric field (up to $E_r \sim +10$kV/m) is derived for radii up to about r/a=0.5 which reduces strongly the electron heat flux to the $\sqrt{\nu}$ regime. Indeed the steep T_e gradients cannot be explained for vanishing E_r, resembling a 1/ν-regime, as with E_r=0 these gradients result in electron heat fluxes ($Q_e+\Gamma_e T_e$) that clearly exceed the applied heating power (by up to a factor of 6). The CERC conditions are confirmed from first E_r measurements with correlation reflectometry (23) and from the Doppler shift of Ar impurity lines in X-ray imaging spectroscopy (24): Both show a change in the sign of the core radial electric field $E_r(r)$ from negative values (ion root) at about r/a>0.4 to positive values (electron-root) (~+10kV/m) in the inner core (25).

The existence of a $\sqrt{\nu}$ regime with dominant E_r is confirmed from a configuration scan where the effective helical ripple ε_{eff} as a course measure for the remaining poloidal variation of B has been varied from 0.7% to 1.4%. Contrary to the expectations from the 1/ν regime where the diffusion coefficient scales strongly with ε_{eff} as $D_{1/\nu} \sim \varepsilon_{eff}^{3/2} \cdot n^{-1} \cdot T^{7/2}$ there are no significant T_e-profile changes in the region of strong T_e-gradients. This is consistent with the expectation for $\sqrt{\nu}$ -regime with finite E_r where the dependency on ε_{eff} vanishes as $D_{\sqrt{\nu}} \sim n^{1/2} T^{5/4} Er^{-3/2}$ (25).

But even the maximum neoclassical fluxes do not carry the launched heating power, e.g. in Fig. 3 achieve ~1.1 MW in maximum for P_{ECRH}=2.0MW indicating residual fluxes may be carried by turbulence, radiation and CX neutrals. These fluxes prevail in particular in the outer part of the confinement region where the neoclassical ambipolarity condition predicts ion root conditions with negative E_r in agreement with measurements (23).

Power step experiments varying 0.6 MW < P_{ECRH}< 4 MW (25) show that the residual fluxes increase with increasing P_{ECRH} indicating a power degradation of confinement. Global figures for the energy confinement time for power step experiments indicate τ_E to scale like $\tau_E \sim P^{-0.5\pm 0.1}$ which is compliant with plateau scaling ($P^{-0.6}$) at higher collisionality but with the tendency of lower power degradation (25). This finding is not in contradiction to the observation that the CERC region grows with heating power, since the outer region of the plasma contains the main fraction (typically >70%) of the total confined energy.

4.4 First observations on transport beyond neoclassics

Stationary and dynamic transport studies were conducted together with the flexible ECRH system with its option for on- and off-axis heating, power steps and power modulation (7, [26]). Albeit T_e and T_i profiles are highly reproducible for the same conditions a thorough transport analysis is hampered by the uncontrolled density and the lack of information on Z_{eff}.

-> In the small configuration scan shifting the 5/6 rational (islands) radially inward the T_e-profiles did not indicate show an influence of island location on local transport.

-> With off-axis heating the T_e profiles broaden considerably (Fig. 4) as expected for a local transport model. In the ECE spectra associated with strong off-axis heating crash events are observed with inversion radius around 3 keV (13).

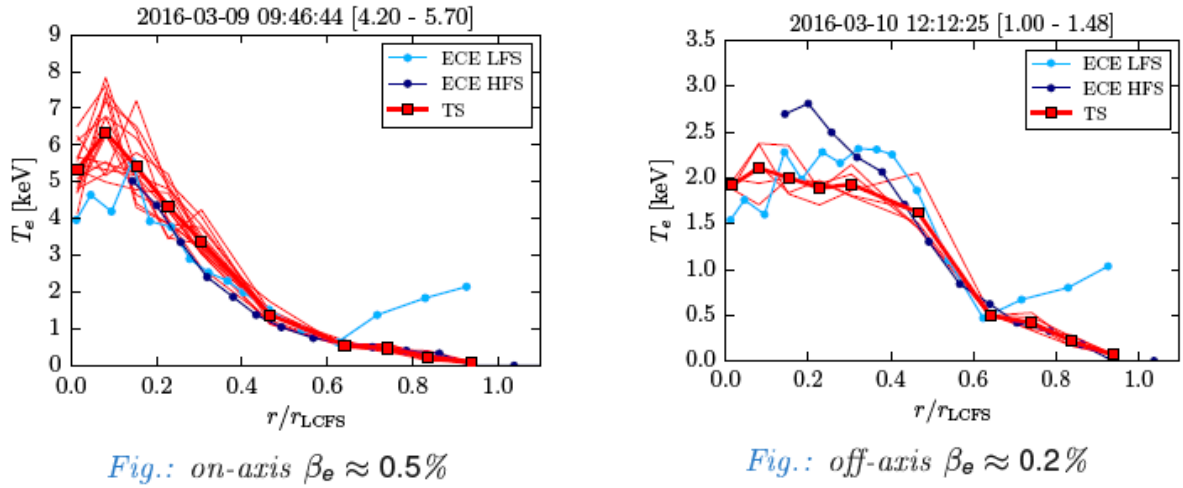

Fig. 4: Temperature profiles with on- and off axis heating.

-> Heatwave propagation experiments, with on- and off-axis power modulation of the gyrotrons, allow for the determination of the ECRH power deposition profiles as well as for dynamic electron transport studies that are presented in (26, 27).

-> The plasmas display a variety of dynamic phenomena such as a nearly coherent activity with frequency around 7 to 10 kHz located ~r/a=0.5 in several scenarios and individual transport events which are candidates to affect confinement.

Conclusion

A first glance on confinement in the optimized stellarator W7-X exceeds expectations. Energy confinement times of the order of 150 ms are obtained as extrapolated from ISS04 scaling with configuration factor 1.0 (20) although the limiter configuration in a device with unprotected metal walls, thus large impurity content and anticipated CX-losses, do not yet allow to conclude on stellarator optimization. The T_e-profiles respond to on- and off-axis ECR heating correspondingly. The inner half of the plasma agrees with Core Electron Root Confinement in agreement with calculations and provides a first access for a comparison with the expectations for optimized stellarator.

Acknowledgement

This work has been carried out within the framework of the EUROfusion Consortium and has received funding from the Euratom research and training programme 2014-2018 under grant agreement No 633053. The views and opinions expressed herein do not necessarily reflect those of the European Commission.

References

[1] J. Nührenberg, Phys. Lett. A **114**, 129 (1986), G. Grieger, G. et al Phys. Fluids B 4, (1992) 2081

[2] T. S. Pedersen et al., Nucl. Fusion 55 (2015) 126001, T. Klinger et al. , submitted to Plasma Phys. Contol Fusion, R. Wolf et al, this conference

[3] e.g. Y. Feng et al. Plasma Phys. Control. Fusion **53** (2011) 024009

[4] M. Hirsch et al. 2008 Plasma Phys Control Fus. 053001

[5] M. Yokoyama et al. Nuclear Fusion, 47, 9, 1213 (2007).

[6] M. Otte et al. Plasma Phys. Control. Fusion **58** (2016) 064003

[7] S. Marsen et al. Proc. 43rd EPS Conf. 4.7 - 8.7.2016, Leuven, Belgium, P4.002

[8] T. Wauters et al. Proc. 43rd EPS Conf. 4.7 - 8.7.2016, Leuven, Belgium, P4.047

[9] B. Buttenschön et al. Proc. 43rd EPS Conf. 4.7 - 8.7.2016, Leuven, Belgium, P4.012

[10] P. Kornejew et al. to be published, J. Knauer et al 2016, EPS Leuven, Belgium, P4.017

[11] K. Rahbarnia et al. Proc. 43rd EPS Conf. 4.7 - 8.7.2016, Leuven, Belgium, P4.011

[12] H. Thomsen et al. Proc. 43rd EPS Conf. 4.7 - 8.7.2016, Leuven, Belgium, P4.010

[13] M. Hirsch et al. Proc. 43rd EPS Conf. 4.7 - 8.7.2016, Leuven, Belgium, P4.007

[14] E. Pasch et al. Proc. 43rd EPS Conf. 4.7 - 8.7.2016, Leuven, Belgium, P4.016

[15] A. Langenberg et al. Proc. 43rd EPS Conf. 4.7 - 8.7.2016, Leuven, Belgium, P4.014

[16] D. Zhang et al. Proc. 43rd EPS Conf. 4.7 - 8.7.2016, Leuven, Belgium, P4.015

[17] S. Bozhenkov et al. Proc. 43rd EPS Conf. 4.7 - 8.7.2016, Leuven, Belgium, O2.106

[18] H. Niemann et al. 2016 EPS, P4.0005, G. A. Wurden et al. this conference EX/P5-7

[19] G. Fuchert et al., to be published

[20] H. Yamada et al, Nucl. Fus. 45 1684 (2005).

[21] L. Stephey et al. 2016 APS, to be published in Phys. of Plasmas

[22] S.P. Hirshman et al., Phys. Fluids 29 (1986) 2951

[23] A. Krämer Flecken et al., this conference

[24] N. Pablant et al. Proc. 43rd EPS Conf. 4.7 - 8.7.2016, Leuven, Belgium, P4.013

[25] A. Dinklage et al. Proc. 43rd EPS Conf. 4.7 - 8.7.2016, Leuven, Belgium, O2.107

[26] U. Höfel et al, Proc. 43rd EPS Conf. Leuven, P4.008

[27] G. M. Weir et al Proc. 43rd EPS Conf. Leuven P4.009